






^{13}C NMR evidence for strong electron correlation and antiferromagnetic order in the single-component molecular material $\text{Pd}(\text{tmdt})_2$ Taiga Takahashi,¹ Keishi Sunami ,^{1,*} Kazuya Miyagawa ,¹ Rina Takagi,^{1,2} Biao Zhou ,³
Akiko Kobayashi ,³ and Kazushi Kanoda ^{1,†}¹*Department of Applied Physics, University of Tokyo, Bunkyo-ku, Tokyo 113-8656, Japan*²*Institute of Engineering Innovation, University of Tokyo, Bunkyo-ku, Tokyo 113-8656, Japan*³*Department of Chemistry, College of Humanities and Sciences, Nihon University, Setagaya-ku, Tokyo 156-8550, Japan*

(Received 27 April 2019; revised manuscript received 4 July 2019; published 8 August 2019)

We performed ^{13}C NMR measurements on the single-component molecular material $\text{Pd}(\text{tmdt})_2$ to reveal the nature of the electronic phase. For the conducting state above 200 K, the analyses using the paramagnetic shift and the nuclear spin-lattice relaxation rate find large values of the Korringa ratio indicative of highly enhanced antiferromagnetic fluctuations. A clear NMR line broadening, indicative of an antiferromagnetic order, occurs at approximately 80 K with a traceable broadening extending up to 140 K, which possibly signifies a minor fraction of a higher-temperature magnetic phase in conjunction with a change in the NMR relaxation curve below 140 K. Comparing the observed spectral profile at 5 K and simulations, the magnetic moment is estimated to be $\sim 0.18\mu_{\text{B}}/\text{tmdt}$. The present results show that $\text{Pd}(\text{tmdt})_2$ is a Mott insulator situated near the Mott transition and hosts strong exchange interactions that give an antiferromagnetic order at an extremely high transition temperature among molecular materials.

DOI: [10.1103/PhysRevB.100.075117](https://doi.org/10.1103/PhysRevB.100.075117)**I. INTRODUCTION**

Strongly correlated electron systems exhibit a variety of fascinating phenomena [1,2] such as metal-insulator Mott transitions, charge ordering, and quantum spin liquids. $M(\text{tmdt})_2$ is a planar molecule with a metal ion M coordinated by ligands of tmdt (trimethylenetetrafulvalenedithiolate) from both sides [Fig. 1(a)] and constructs single-component molecular conductors without counteranions or cations [Figs. 1(b) and 1(c)], in contrast to most molecular conductors, which are composed of various kinds of molecules [3–8]. The electronically active orbitals in $M(\text{tmdt})_2$ are the $d_{p\sigma}$ orbital located centered at the M ion and the $p\pi$ orbitals extended over the tmdt ligands. The interplay between these orbitals with different characters generates a variety of electronic states; in particular, different kinds of correlated electron phases were predicted to emerge by replacing M [9,10] and indeed were found experimentally [8,11–14]. For $M = \text{Cu}$, the energy level of the $d_{p\sigma}$ orbital is close to that of the $p\pi$ orbitals, leading to a multiorbital Mott insulator, in which an antiferromagnetic (AF) order of the $d_{p\sigma}$ spins coexists with spin singlets of the $p\pi$ spins [7,11,12]. For $M = \text{Ni}$, Pt , and Pd , only the $p\pi$ orbitals contribute to the overlapping conduction and valence bands because the energy level of the $d_{p\sigma}$ orbital is separated above from that of the $p\pi$ orbitals located at the Fermi level [6,8,15] [Fig. 1(d)]. Among the three members, $\text{Ni}(\text{tmdt})_2$ and $\text{Pt}(\text{tmdt})_2$ are moderately correlated paramagnetic metals [3,6,16]. However, $\text{Pd}(\text{tmdt})_2$ shows different transport and

magnetic properties; the resistivity is almost flat in temperatures of 150–300 K and increases upon cooling below 150 K, with an extremely small activation energy of 3–9 meV [8]. Concerning magnetism, the electron spin resonance signal intensity drops [8], and the ^1H nuclear magnetic resonance (NMR) spectrum is broadened below 100 K [14], indicating an AF spin order. The insulating behavior and AF order at low temperatures suggest that $\text{Pd}(\text{tmdt})_2$ is an AF Mott insulator.

A remarkable feature of $\text{Pd}(\text{tmdt})_2$ is that it has one electron per tmdt ligand, unlike the representative organic Mott insulator, $\kappa\text{-(BEDT-TTF)}_2\text{Cu}[\text{N}(\text{CN})_2]\text{Cl}$ (hereafter $\kappa\text{-Cl}$) with one hole per dimer of bis(ethylenedithio)tetrathiafulvalene (BEDT-TTF) molecules [17]. Thus, $\text{Pd}(\text{tmdt})_2$ is expected to have a stronger magnetic exchange interaction than $\kappa\text{-Cl}$ because the exchange interaction in $\text{Pd}(\text{tmdt})_2$ is determined by the transfer integral t between tmdt, whereas the exchange interaction in dimer Mott insulators such as $\kappa\text{-Cl}$ is determined by the interdimer transfer integral, which is roughly half of t .

The AF order in $\text{Pd}(\text{tmdt})_2$ is also indicated by the ^1H NMR spin-lattice relaxation rate $1/T_1$, which forms a peak at ~ 50 K [14]. However, the peak temperature is much lower than the onset temperature of the spectral broadening, and the observed peak is broad, unlike the divergent behavior seen in typical AF transitions [18], meaning a distribution of the AF transition temperature possibly due to disorder in $\text{Pd}(\text{tmdt})_2$ [8,14]. The small activation energy of 3–9 meV at low temperature may also be caused by disorder, as the resistivity in the Mott insulator, $\kappa\text{-Cl}$, situated near a Mott transition is considerably reduced by x-ray irradiation, which introduces disorder to the sample [19]. In the present study, to investigate in depth the $p\pi$ electronic states in $\text{Pd}(\text{tmdt})_2$, we observe the NMR signals at the central double-bonded ^{13}C sites in the

*sunami@mdf2.t.u-tokyo.ac.jp

†kanoda@ap.t.u-tokyo.ac.jp

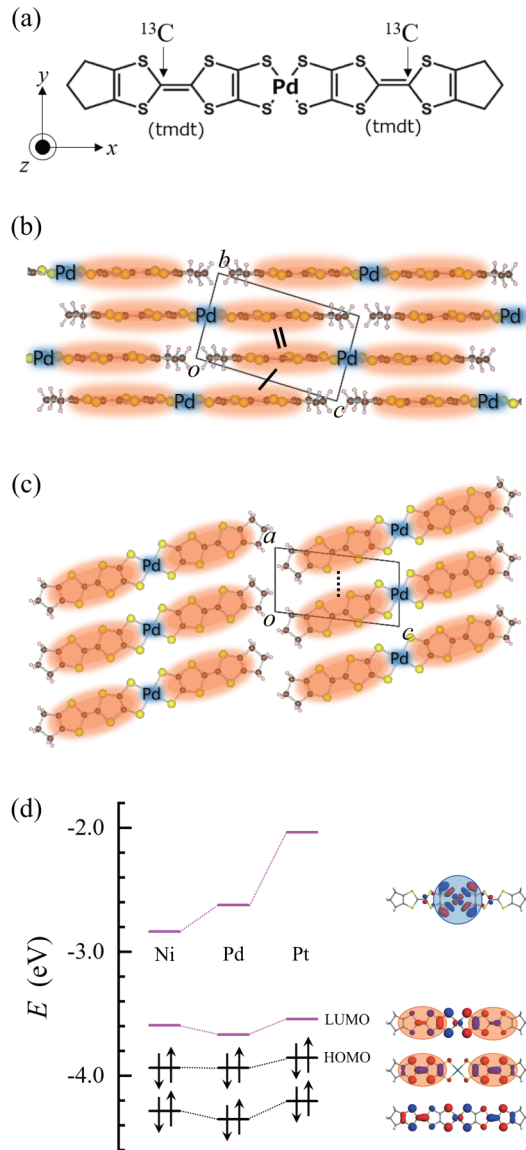


FIG. 1. (a) Molecular structure of Pd(tmdt)₂. The arrows indicate the carbon sites enriched by ¹³C isotopes to 99 at. %. The molecular principal axes, which are identical to the principal axes of the hyperfine coupling tensor at the ¹³C sites, are represented by *x*, *y*, and *z*. Crystal structures of Pd(tmdt)₂ viewed along (b) the *a* axis and (c) the *b* axis [8]. The double and single lines in (b) and the dotted line in (c) indicate the nearest-, second-nearest-, and third-nearest-neighbor tmdt pairs, respectively. The orange (blue) regions depict the spatial extension of the *pπ* (*dpσ*) orbitals. (d) Energy levels of molecular orbitals in *M*(tmdt)₂ (*M* = Ni, Pd, and Pt) obtained by DFT molecular orbital calculations [6,8,15].

tmdt ligands [Fig. 1(a)] because the ¹³C NMR is superior to ¹H NMR for probing the *pπ* electronic states in two respects; one is that the ¹³C nuclei have stronger hyperfine coupling with the *pπ* spins than ¹H nuclei because the population of *pπ* electrons is concentrated at the central double-bonded carbon sites on tmdt [8], and the other is that ¹H NMR $1/T_1$ probes not only electron spin fluctuations but, inevitably, molecular motions of trimethylene on the edge of tmdt, as demonstrated in Ni(tmdt)₂ and Pt(tmdt)₂ [16]. Indeed, ¹H

NMR $1/T_1$ forms a moderate peak at ~ 200 K in addition to the broad peak around 50 K associated with the AF order in Pd(tmdt)₂ [14], suggesting that the molecular motions dominate $1/T_1$ at high temperatures and mask the electronic contribution to $1/T_1$. Thus, in the present work, we performed the ¹³C NMR study, which is expected to probe the precise nature of *pπ* electrons in Pd(tmdt)₂ by resolving the paramagnetic shift, evaluating the NMR enhancement factor characterizing the type and strength of spin correlation, and determining the AF moments.

II. EXPERIMENT

The ¹³C NMR measurements were performed on fine polycrystals of Pd(tmdt)₂, in which the outer carbon of the central double-bonded carbons in tmdt was selectively enriched by ¹³C isotopes to 99% [Fig. 1(a)]. The NMR spectra were obtained by the fast Fourier transformation of the spin-echo signals following the $(\pi/2)_x - (\pi)_x$ pulse sequence. The $\pi/2$ pulse width was 1.3–2.0 μ s. We used the ¹³C signal of TMS (tetramethylsilane) as the shift origin of NMR spectra. In general, the relaxation of nuclear magnetization is characterized by the single-exponential function, $M(\infty) - M(t) \propto \exp[-(t/T_1)]$, where T_1 is the nuclear spin-lattice relaxation time and $M(t)$ is the nuclear magnetization at a time t after its saturation caused by the so-called rf comb pulse. In the case of polycrystalline samples, the T_1 values are distributed in a range due to the different orientation of each crystal against the field direction, and thus, we determined $1/T_1$ by fitting the stretched exponential function, $M(\infty) - M(t) \propto \exp[-(t/T_1)^\beta]$, to the relaxation data usually employed, where the exponent β ($0 < \beta \leq 1$) characterizes the degree of distribution in T_1 .

III. RESULTS AND DISCUSSION

A. Paramagnetic state at high temperatures

Figure 2(a) shows the ¹³C NMR spectra of polycrystalline Pd(tmdt)₂ under a magnetic field of 6 T at various temperatures. As seen in the expanded figures [Fig. 2(b)], the spectral shapes are asymmetric near room temperature, reflecting the paramagnetic shift tensor with a uniaxial symmetry characteristic of the *pπ* orbital in the tmdt ligands. Upon cooling, the line shape becomes symmetric and is broadened, indicating that the inhomogeneous local fields are generated at ¹³C sites due to the AF order of *pπ* electrons, as discussed in Sec. III B.

We try to fit the asymmetric spectra observed at high temperatures by the spectral function expected for polycrystals with the paramagnetic shift tensor of a uniaxial symmetry. It is expressed by the sum of the spectral contributions from each grain oriented arbitrarily against a magnetic field $\mathbf{H}_0 = H_0(\cos\phi\sin\theta, \sin\phi\sin\theta, \cos\theta)$ described in spherical coordinates (θ, ϕ) . The spectral position for each grain is given by $\delta(\theta, \phi) = \delta_{xx}\sin^2\theta\cos^2\phi + \delta_{yy}\sin^2\theta\sin^2\phi + \delta_{zz}\cos^2\theta$ with the principal values of the shift tensor (δ_{xx} , δ_{yy} , δ_{zz}), where *x*, *y*, and *z* are the molecular principal axes as defined in Fig. 1(a). Assuming that the spectral shape for each grain is described by the Lorentzian function with the inhomogeneous width Δ ,

the spectral function $F(\nu)$ is expressed by

$$F(\nu) = p \iiint \frac{\Delta}{(\delta_{xx}\sin^2\theta\cos^2\phi + \delta_{yy}\sin^2\theta\sin^2\phi + \delta_{zz}\cos^2\theta - \nu)^2 + \Delta^2} \sin\theta d\theta d\phi, \quad (1)$$

where p is the normalization factor. The shift tensor is composed of the chemical shift and the paramagnetic shift. Both shifts can be divided into isotropic and anisotropic parts. Thus, the total shift tensor of Pd(tmdt)₂ is written as

$$\begin{pmatrix} \delta_{xx} & & \\ & \delta_{yy} & \\ & & \delta_{zz} \end{pmatrix} = 126 + \begin{pmatrix} 47 & & \\ & -4.4 & \\ & & -42.8 \end{pmatrix} + K_{\text{iso}}(T) + K_{\text{aniso}}(T) \begin{pmatrix} -1 & & \\ & -1 & \\ & & 2 \end{pmatrix}. \quad (2)$$

The first and second terms are the isotropic and anisotropic components of the chemical shift. For those, we used the chemical shift tensor of a spin-gapped Mott insulator, Zn(tmdt)₂ [13], because the low-temperature shift for Zn(tmdt)₂ is attributed to the chemical shift due to the nonmagnetic nature of the ground state [5,13]. The third and fourth terms are the isotropic and anisotropic components of the paramagnetic shift to be determined by the fitting. The anisotropic part of the paramagnetic shift tensor is assumed to be uniaxial around the z axis because the carbon-site $2p_z$ orbitals, which constitute the $p\pi$ orbitals on tmdt, are uniaxial around the z axis. The inhomogeneous width Δ is given by $\Delta = \Delta_0 + \Gamma|K_{\text{iso}} - K_{\text{aniso}}\sin^2\theta\cos^2\phi - K_{\text{aniso}}\sin^2\theta\sin^2\phi + 2K_{\text{aniso}}\cos^2\theta|$, which consists of the constant term Δ_0 and the second term proportional to the paramagnetic shift with the prefactor Γ . Thus, the fitting parameters are K_{iso} , K_{aniso} , p , Δ_0 , and Γ .

First, we fitted the spectrum for 279 K with the five parameters and could reproduce the spectral feature well, as shown in Fig. 2(b). Then, in the spectral fitting for other temperatures, we fixed $K_{\text{aniso}}/K_{\text{iso}}$ and Δ_0 to 0.79 and 3.0 ppm, respectively, which are the values obtained from the fitting for 279 K; these values are expected to be independent of temperature. Thus, the fitting parameters are reduced to K_{iso} , p , and Γ . As shown in Fig. 2(b), the observed spectra above 100 K are well fitted by Eq. (1), indicating that the shapes of the spectra are attributed to the uniaxial nature of $p\pi$ orbitals. These spectral fittings yield the temperature dependence of the fitting parameters; in particular, we show the temperature profile of K_{iso} in Fig. 3(a) along with those for $M = \text{Ni}$ and Pt compounds [16]. For reference, we also display, on the right axis, the scale of the spin susceptibility χ , evaluated through

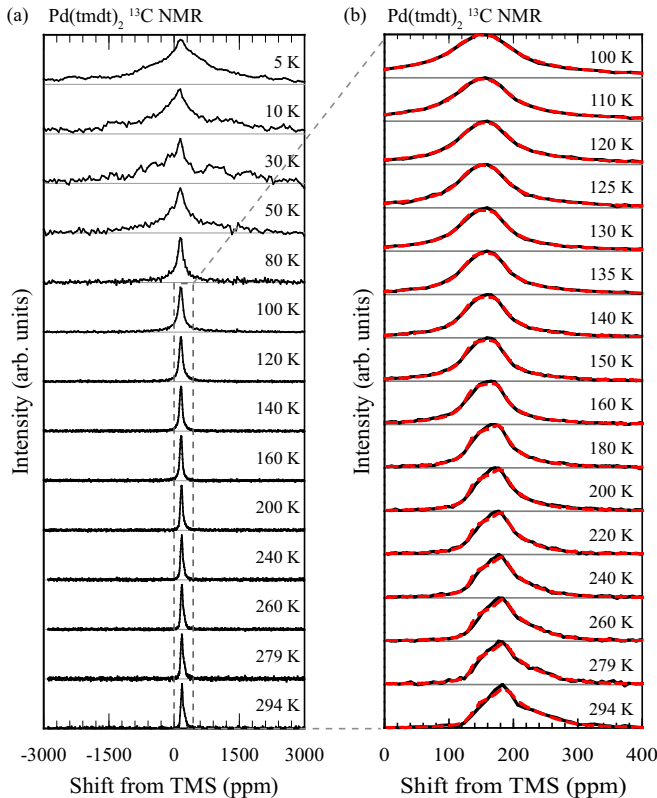


FIG. 2. (a) ¹³C NMR spectra for Pd(tmdt)₂. (b) Detailed temperature dependence of the NMR spectra at 100–294 K. The red dashed lines are fitting curves represented by Eq. (1).

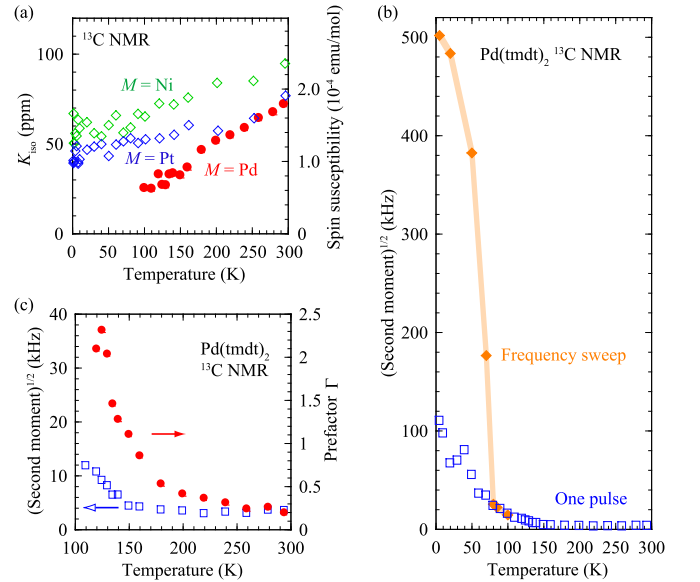


FIG. 3. (a) Temperature dependence of the isotropic part of the paramagnetic shift K_{iso} for $M = \text{Pd}$ (the present result) and Ni and Pt (reproduced from Ref. [16]). The right axis denotes the scale of spin susceptibility χ evaluated through $\chi = K_{\text{iso}}/a_{\text{iso}}$, with $a_{\text{iso}} = 4.5 \text{ kOe}/(\mu_B \text{ tmdt})$, the average of the a_{iso} values for $M = \text{Ni}$ and Pt [16] (see text). (b) Square root of the second moment of NMR spectra obtained by the one-pulse (blue open squares) and frequency-sweep (orange solid diamonds) measurements as a function of temperature (see text). (c) Temperature dependence of the prefactor Γ (red solid circles) deduced in spectral fittings (see text). The square root of the second moment [blue open squares plotted in (b)] is also shown for a detailed comparison with Γ .

$\chi = K_{\text{iso}}/a_{\text{iso}}$, with the value of $a_{\text{iso}} = 4.5 \text{ kOe}/(\mu_{\text{B}} \text{ tmdt})$, which is the average of 3.9 and 5.1 $\text{kOe}/(\mu_{\text{B}} \text{ tmdt})$ for $M = \text{Ni}$ and Pt , respectively [16]. The χ value for $\text{Pd}(\text{tmdt})_2$ is comparable to those for $\text{Ni}(\text{tmdt})_2$ and $\text{Pt}(\text{tmdt})_2$ at room temperature but decreases with temperature more steeply than the latter two. This material dependence is reminiscent of the systematic variation of χ for $\kappa\text{-(BEDT-TTF)}_2X$ ($X = \text{Cu}(\text{NCS})_2$, $\text{Cu}[\text{N}(\text{CN})_2]\text{Br}$, and $\text{Cu}[\text{N}(\text{CN})_2]\text{Cl}$, hereafter $\kappa\text{-NCS}$, $\kappa\text{-Br}$, and $\kappa\text{-Cl}$, respectively) situated near the Mott transition. $\kappa\text{-NCS}$ is a metal located well off the Mott boundary, $\kappa\text{-Br}$ resides more closely to the boundary, and $\kappa\text{-Cl}$ is marginally in the Mott insulating region [20]. The values of χ are temperature insensitive and similar in magnitude for all three salts above 200 K, whereas χ decreases with temperature below 100 K more steeply in the ascending order of $\kappa\text{-NCS}$, $\kappa\text{-Br}$, and $\kappa\text{-Cl}$, indicating that χ is suppressed at low temperatures near the Mott transition. Likewise, the material dependence of χ in $M(\text{tmdt})_2$ with $M = \text{Ni}$, Pt , and Pd can be addressed as the behavior near the Mott transition. The magnitude of χ for $M(\text{tmdt})_2$ is roughly half of that for $\kappa\text{-(BEDT-TTF)}_2X$, possibly reflecting the difference in the density of states between the two families; note that $\text{Ni}(\text{tmdt})_2$ is a semimetal with the Fermi level located at the valley in the density-of-states profile [21].

B. Antiferromagnetic state at low temperatures

Figure 3(b) shows the second moment of the spectra shown in Fig. 2(a), which increases below 140–150 K. We note that these spectra are obtained from the echo signal acquired with a single pulse, whose width limits the range of spectral frequencies. The frequency ν profile of the input radio wave pulse has a maximum intensity at the input radio wave frequency ν_0 and fades away as ν deviates from ν_0 ; for example, with a pulse width of $2 \mu\text{s}$ as employed in the present study, the spectral intensity should decay to 67% of the central value at $\nu_0 \pm 240 \text{ kHz}$ [22], which corresponds to approximately $\pm 3700 \text{ ppm}$ on the horizontal axis in Fig. 2. This value is comparable to the width of the spectrum observed at low temperatures [Fig. 2(a)], implying that the observed spectral width is limited by the experimental pulse width and the entire spectrum is not properly acquired with the single pulse at low temperatures. Thus, we measured the NMR signals with ν_0 shifted at intervals of 25–200 kHz in the range of 84.0–87.4 MHz under a magnetic field of 8 T and constructed the whole profiles of spectra below 100 K by connecting the spectra obtained at each ν_0 . In Fig. 3(b), we also plot the second moments of the thus obtained spectra, which agree with those obtained by the one-pulse method in $80 < T < 100 \text{ K}$ but drastically increase below 80 K. We note that a moderate line broadening starts at $\sim 140 \text{ K}$, and as discussed later, the temporal profile of NMR relaxation changes below 140 K, which can be another signature of a magnetic ordering. These experimental features suggest an inhomogeneous AF order, which onsets at approximately 140 K, followed by the ordering in a major fraction of the sample around 80 K. We note the contribution of the critical slowing down of the AF fluctuations to the spectral width in what follows. In Fig. 3(c), we show the temperature profile of Γ , which characterizes the spectral width of electron spin origin in each grain, deduced

from the spectral fittings in Sec. III A. The Γ value is enhanced upon cooling from temperatures much higher than 140 K, which possibly indicates the growth and slowing down of AF fluctuations toward the AF transition. This behavior is not clearly visible in the temperature dependence of the second moment in the same temperature range [Fig. 3(c)] because the Γ value is directly related to the spectral width for each grain, whereas the main contribution to the second moment is the distribution of the spectral position from grain to grain.

As shown in the ^{13}C NMR study of $\kappa\text{-Cl}$ [23], the Dzyaloshinskii-Moriya (DM) interactions induce staggered moments under an applied field; they can cause NMR line broadening for a polycrystalline sample. In the present system, tmdt ligands where spins reside have inversion centers in the nearest-neighbor pair and in the second-nearest-neighbor pair [see Fig. 1(b)]. Although the third-nearest neighbor is not mutually related by inversion, its geometrical asymmetry is not significant, as seen in Fig. 1(c). Thus, the DM interactions should not be effective in $\text{Pd}(\text{tmdt})_2$.

The spectral profile at low temperatures reflects the local-field distribution in the AF ordered state. Figure 4(a) shows the spectrum at 5 K, acquired with the “frequency shift” under 8 T. To evaluate the size of the AF moments from the spectral profile, we simulated the spectral shape expected for polycrystals, in which moments of $1\mu_{\text{B}}/\text{tmdt}$ are ordered, under the following assumptions: (i) the magnetic moments are directed in the plane perpendicular to the external magnetic field $\mathbf{H}_0 = H_0(\cos\phi\sin\theta, \sin\phi\sin\theta, \cos\theta)$ due to the spin flop, and (ii) the magnetic anisotropy is ignored. Thus, the magnetic moment s is expressed as $s/s = (\cos\phi\cos\theta\cos t - \sin\phi\sin t, \sin\phi\cos\theta\cos t + \cos\phi\sin t, -\sin\theta\cos t)$, where s is $|s|$ and t ($0 \leq t < 2\pi$) characterizes the direction of the moments in the plane. (iii) In addition, we assumed that the hyperfine coupling tensor \mathbf{A} at the ^{13}C nuclei has uniaxial anisotropy for the z axis, as mentioned in Sec. III A; namely, \mathbf{A} is described as

$$\mathbf{A} = \begin{pmatrix} a_{xx} & & \\ & a_{yy} & \\ & & a_{zz} \end{pmatrix} = a_{\text{iso}} + a_{\text{aniso}} \begin{pmatrix} -1 & & \\ & -1 & \\ & & 2 \end{pmatrix}, \quad (3)$$

and (iv) we used the hyperfine coupling constants, $(a_{\text{iso}}, a_{\text{aniso}}) = (4.5, 3.55) \text{ kOe}/(\mu_{\text{B}} \text{ tmdt})$, which are the averages of the values for $\text{Ni}(\text{tmdt})_2$ and $\text{Pt}(\text{tmdt})_2$ [16]; note that the ratio $a_{\text{aniso}}/a_{\text{iso}} = 0.79$ is in good agreement with the above-mentioned shift ratio, $K_{\text{aniso}}/K_{\text{iso}} = 0.79$, for the present system. The \mathbf{H}_0 -parallel component of the local field generated by a magnetic moment of $1\mu_{\text{B}}/\text{tmdt}$, $h(\theta, \phi, t)$, is given by $h = \mathbf{H}_0 \cdot \mathbf{A} \cdot s/H_0s$. For the polycrystalline sample, we need to sum up the spectral contributions from grain to grain, in which t is also averaged uniformly in $0 \leq t < 2\pi$; thus, the spectral function $F(\nu)$ is described as in the case with Eq. (1),

$$F(\nu) = \iiint \frac{\Delta}{[\nu - \gamma h(\theta, \phi, t)/2\pi]^2 + \Delta^2} \sin\theta d\theta d\phi dt, \quad (4)$$

where γ is the gyromagnetic ratio of ^{13}C nuclei. The simulated spectra for $1\mu_{\text{B}}/\text{tmdt}$ with $\Delta = \Delta_0 + \Gamma\gamma h(\theta, \phi, t)$ are

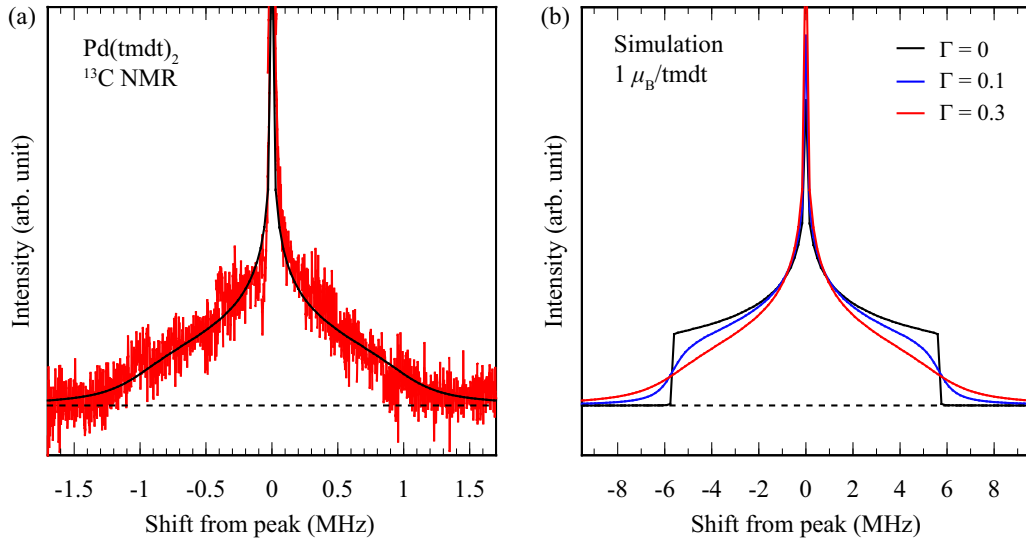


FIG. 4. (a) ¹³C NMR spectrum of Pd(tmdt)₂ at 5 K under a magnetic field of 8 T. The spectrum is constructed by connecting the partial spectra acquired under the radio wave frequency ν_0 , which is shifted at intervals of 25–200 kHz in the range of 84.0–87.4 MHz. The black line is a simulated spectrum based on Eq. (4) with $\Delta_0 = 0.004$ MHz and $\Gamma = 0.3$ for $0.18\mu_B/\text{tmdt}$. (b) Spectral simulations based on Eq. (4) with $\Delta_0 = 0.004$ MHz and $\Gamma = 0, 0.1, \text{ and } 0.3$ for $1\mu_B/\text{tmdt}$.

shown in Fig. 4(b). The Γ value characterizes the degree of distribution in the magnitude of the magnetic moments. For $\Gamma = 0$, the simulated spectrum has clear edges at ± 6 MHz, and the edge structures become gentle with increasing Γ . The observed spectral shape is well reproduced by the simulation with $\Gamma = 0.3$ for $0.18\mu_B/\text{tmdt}$ [Fig. 4(a)], suggesting that the local moments are distributed by $\sim 30\%$ around the mean value of $0.18\mu_B/\text{tmdt}$. The sharp central peak in the spectrum comes from the spin flop because the powder spectrum in the nonflopped case is analytically shown to have a rectangular shape with no anomaly around the origin. [We note that the central peak in Fig. 4(a) corresponds to the broad line in Fig. 2(a).] Conceivable origins for the small and distributed magnetic moments are the following; one is that the localization of electrons is weak because Pd(tmdt)₂ is situated close to the Mott transition, as discussed later in detail, and the other is the effect of disorder, which drives the Mott-localized electrons into more delocalized states, as suggested in earlier works [19,24], and makes the exchange interactions weakened and distributed.

The temperature dependence of the nuclear spin-lattice relaxation rate $1/T_1$ has a moderate peak structure around 70–100 K [Fig. 5(a)], indicative of the critical slowing down of AF fluctuations, which is in agreement with the AF transition temperature of 80 K determined by the steep increase of the total second moment; however, the peak is not as divergent as expected for the conventional AF transitions [25], possibly suggesting that the transition temperature is distributed due to disorder [8,14], which also explains the difference between the peak temperature of $1/T_1$, 70–100 K, and the onset of line broadening, 150 K. The exponent β in the stretched exponential fitting of the nuclear relaxation curve is also informative regarding inhomogeneity. The β values are in the range of 0.8–0.9 at $140 < T < 294$ K; the small deviation from unity is very likely due to the distribution of $1/T_1$ from crystal to crystal, each of which is oriented randomly against the applied

field in the polycrystalline sample and exhibits orientation-dependent $1/T_1$ owing to the anisotropic hyperfine coupling tensor. The deviation increases at lower temperatures below 140 K [see the inset of Fig. 5(a)], signifying an additional distribution that starts at 140 K. All these results suggest that the AF transition onsets at 140 K and proceeds in a major part of the sample volume at 80 K.

C. Evaluation of electron correlation in the high-temperature itinerant regime

Above 200 K, the ¹³C NMR $1/T_1$ varies superlinearly with temperature [Fig. 5(a)], in contrast to a peak formation of ¹H NMR $1/T_1$ around 200 K [14], which arises from the molecular motion commonly in isostructural Ni(tmdt)₂ and Pt(tmdt)₂ [16]. Thus, the ¹³C NMR $1/T_1$ probes the $p\pi$ electronic state at high temperatures in Pd(tmdt)₂. Considering that the paramagnetic shift decreases with temperature instead of a constant [Fig. 3(a)], the $1/T_1$ and shift behaviors qualitatively comply with Korringa’s law, being consistent with the weakly metallic behavior in resistivity [8] but incompatible with conventional Mott insulators, as discussed in previous sections. A conceivable picture is that Pd(tmdt)₂ is situated near the Mott transition and thus stays in the metal-insulator crossover region at high temperatures. Indeed, ¹³C NMR $1/T_1$ of κ -Cl situated near a Mott localization shows T -linear behavior at high temperatures and undergoes an AF transition at 27 K [25]. Furthermore, we note that the disorder effect discussed above is particularly significant near the Mott transition, where the Mott localization is weakened by disorder [19,24], which is consistent with the present NMR behaviors. A further study under a systematic variation of disorder may be informative.

As seen in Fig. 5(a), the $1/T_1$ values for Pd(tmdt)₂ are larger than for Ni(tmdt)₂ and Pt(tmdt)₂ in the high-temperature itinerant regime even though the paramagnetic

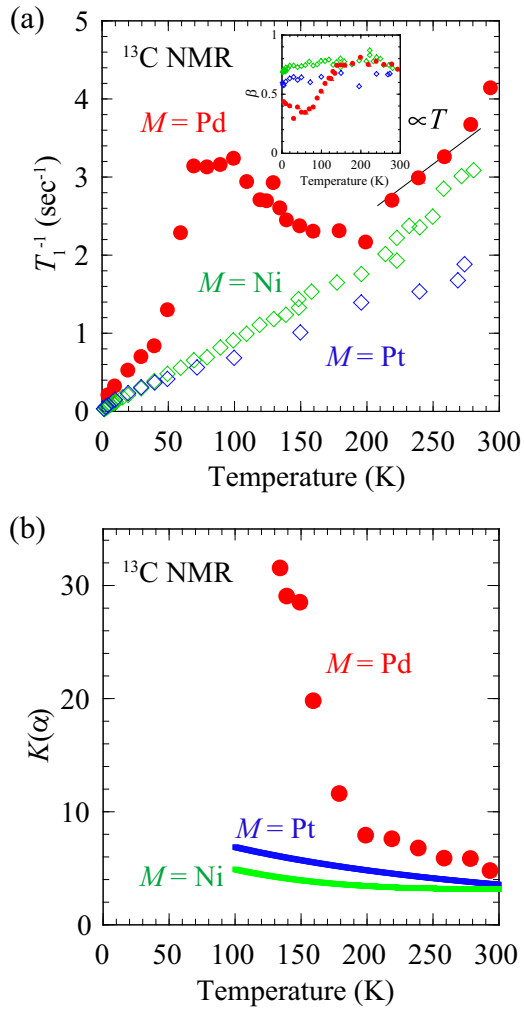


FIG. 5. (a) Temperature dependence of the ^{13}C NMR relaxation rate $1/T_1$ for $M = \text{Pd}$ (the present result) and Ni and Pt (reproduced from Ref. [16]). The inset shows the temperature dependence of the exponent β in the stretched exponential fitting of relaxation curves. (b) Temperature dependence of the Korringa ratio $K(\alpha)$ defined by Eq. (5) for $\text{Pd}(\text{tmdt})_2$ (the present result) and $\text{Ni}(\text{tmdt})_2$ and $\text{Pt}(\text{tmdt})_2$ (reproduced from Ref. [16]).

shift values for the former are smaller than for the latter two, suggesting that $p\pi$ electrons in $\text{Pd}(\text{tmdt})_2$ are more strongly correlated than in $\text{Ni}(\text{tmdt})_2$ and $\text{Pt}(\text{tmdt})_2$. In what follows, we evaluate the electron correlation quantitatively. For polycrystalline samples, Korringa's law for itinerant electron systems is reduced to [25]

$$\frac{1}{i^1 T_1 T} = K(\alpha) \frac{4\pi k_B}{\hbar} \left(\frac{\gamma_n}{\gamma_e} \right)^2 (K_{\text{iso}}^2 + 2K_{\text{aniso}}^2), \quad (5)$$

where $i^1 T_1$ is the relaxation time determined from the initial slope of the relaxation curve of the nuclear magnetization and $K(\alpha)$ is the so-called Korringa ratio, which characterizes the type and strength of spin fluctuations. Note that $1/i^1 T_1$, which is equal to the volume average of $1/T_1$, is employed in Eq. (5) instead of $1/T_1$ in the stretched exponential fitting. If $K(\alpha) = 1$, electron correlations are negligible, whereas $K(\alpha) > 1 (< 1)$ signifies the presence of enhanced antifer-

romagnetic (ferromagnetic) fluctuations. $\text{Pd}(\text{tmdt})_2$ shows a high electrical conductivity of 100 S/cm at room temperature, and its temperature dependence is almost flat at 150–300 K [8]. Thus, we apply Eq. (5) to the present system even though $\text{Pd}(\text{tmdt})_2$ is situated near the Mott transition. Figure 5(b) shows the temperature dependence of $K(\alpha)$ evaluated through Eq. (5) using the experimental data of $i^1 T_1$, K_{iso} , and K_{aniso} for $\text{Pd}(\text{tmdt})_2$. As seen in Fig. 5(b), $K(\alpha)$ is much greater than unity and exceeds the values for $\text{Ni}(\text{tmdt})_2$ and $\text{Pt}(\text{tmdt})_2$ [16] in entire range of temperatures measured, indicating strong AF spin fluctuations in $\text{Pd}(\text{tmdt})_2$. Furthermore, a divergent increase in $K(\alpha)$ with decreasing temperature suggests the critical slowing down of the AF fluctuations toward its long-range order.

We propose two conceivable mechanisms to make a difference in the ground states, the AF Mott insulator for $\text{Pd}(\text{tmdt})_2$ versus the paramagnetic metals for $\text{Ni}(\text{tmdt})_2$ and $\text{Pt}(\text{tmdt})_2$. One is that the highest occupied molecular orbital–lowest unoccupied molecular orbital (HOMO-LUMO) gap in the $\text{Pd}(\text{tmdt})_2$ molecule, 0.268 eV, is smaller than that in the $\text{Ni}(\text{tmdt})_2$ molecule and that in the $\text{Pt}(\text{tmdt})_2$ molecule, 0.343 and 0.312 eV, respectively, as shown in Fig. 1(d) [8]. For $M = \text{Ni}$, Pt , and Pd molecules, HOMO (LUMO) corresponds to the bonding (antibonding) orbital of intramolecular tmdt ligands. Thus, the small HOMO-LUMO gap suggests that the tmdt ligand, rather than the entire $\text{Pd}(\text{tmdt})_2$ molecule, can be viewed as a unit of a molecular orbital composing the HOMO and LUMO bands. In this case, the effective on-site Coulomb interaction U is expected to be large due to the suppression of the spatial extension of the molecular orbital, so that the electron correlations should be more significant in $\text{Pd}(\text{tmdt})_2$ than in $\text{Ni}(\text{tmdt})_2$ and $\text{Pt}(\text{tmdt})_2$. The other is that the nesting between the hole and electron pockets in $\text{Pd}(\text{tmdt})_2$ seems to be better than that in the $M = \text{Ni}$ or Pt compound according to the band structure calculations [8], possibly assisting the Mott instability and the AF ordering in $\text{Pd}(\text{tmdt})_2$.

IV. CONCLUDING REMARKS

We investigated the $p\pi$ electronic states in $\text{Pd}(\text{tmdt})_2$ using the ^{13}C NMR probe. In the itinerant electron regime above 200 K, the NMR spectra of a polycrystalline sample take asymmetric shapes reflecting the uniaxial hyperfine coupling tensor characteristic of the p orbital on the carbon site. The paramagnetic shift, which is deduced from the analysis of the spectra, and nuclear spin-lattice relaxation rate $1/T_1$ yield large Korringa ratios, which exceed the values for the $p\pi$ metallic systems, $\text{Ni}(\text{tmdt})_2$ and $\text{Pt}(\text{tmdt})_2$, demonstrating that $\text{Pd}(\text{tmdt})_2$ hosts highly correlated electrons among this family of materials. The observation of spectral broadening indicates an AF order at 80 K with an inhomogeneous onset at 140 K, which is extremely high among molecular materials and carries moments of $\sim 0.18\mu_B/\text{tmdt}$ at low temperatures. The spectral shape, its temperature dependence, and the temperature profile of $1/T_1$ suggest that the AF order is inhomogeneous or the transition temperature is distributed very likely due to crystal imperfection. We note that the peak temperature of ^1H NMR $1/T_1$ previously measured in different polycrystals is ~ 50 K [14], which is lower than that of ^{13}C NMR

$1/T_1$, ~ 80 K; the difference can be ascribed to the sample dependence of crystalline quality. Considering that even the present sample hosts the inhomogeneous magnetic state, the AF transition may exceed 140 K in the clean limit. These results suggest that $\text{Pd}(\text{tmdt})_2$ is a marginal Mott insulator with strong exchange interactions. It is an intriguing issue to cause the Mott transition in $\text{Pd}(\text{tmdt})_2$ using pressure and see what kind of electronic phases result there.

ACKNOWLEDGMENTS

This work was supported by the JSPS Grants-in-Aid for Scientific Research (S) (Grants No. 25220709 and No. 18H05225) and for Scientific Research (C) (Grants No. 17K05846 and No. 17K05532) and by the Murata Science Foundation.

T.T. and K.S. contributed equally to this work.

-
- [1] M. Imada, A. Fujimori, and Y. Tokura, *Rev. Mod. Phys.* **70**, 1039 (1998).
- [2] Y. Zhou, K. Kanoda, and T. K. Ng, *Rev. Mod. Phys.* **89**, 025003 (2017).
- [3] H. Tanaka, Y. Okano, H. Kobayashi, W. Suzuki, and A. Kobayashi, *Science* **291**, 285 (2001).
- [4] H. Fujiwara, Y. Fujishiro, E. Nishibori, M. Sakata, E. Fujiwara, W. Suzuki, A. Kobayashi, M. Takata, and H. Kobayashi, *J. Am. Chem. Soc.* **125**, 1486 (2003).
- [5] K. Yamamoto, E. Fujiwara, A. Kobayashi, Y. Fujishiro, E. Nishibori, M. Sakata, M. Takata, H. Tanaka, Y. Okano, and H. Kobayashi, *Chem. Lett.* **34**, 1090 (2005).
- [6] B. Zhou, A. Kobayashi, Y. Okano, T. Nakashima, S. Aoyagi, E. Nishibori, M. Sakata, M. Tokumoto, and H. Kobayashi, *Adv. Mater.* **21**, 3596 (2009).
- [7] B. Zhou, H. Yajima, A. Kobayashi, Y. Okano, H. Tanaka, T. Kumashiro, E. Nishibori, H. Sawa, and H. Kobayashi, *Inorg. Chem.* **49**, 6740 (2010).
- [8] S. Ogura, Y. Idobata, B. Zhou, A. Kobayashi, R. Takagi, K. Miyagawa, K. Kanoda, H. Kasai, E. Nishibori, C. Satoko, and B. Delley, *Inorg. Chem.* **55**, 7709 (2016).
- [9] S. Ishibashi, K. Terakura, and A. Kobayashi, *J. Phys. Soc. Jpn.* **77**, 024702 (2008).
- [10] H. Seo, S. Ishibashi, Y. Otsuka, H. Fukuyama, and K. Terakura, *J. Phys. Soc. Jpn.* **82**, 054711 (2013).
- [11] R. Takagi, K. Miyagawa, K. Kanoda, B. Zhou, A. Kobayashi, and H. Kobayashi, *Phys. Rev. B* **85**, 184424 (2012).
- [12] R. Takagi, T. Hamai, H. Gangi, K. Miyagawa, B. Zhou, A. Kobayashi, and K. Kanoda, *Phys. Rev. B* **95**, 094420 (2017).
- [13] R. Takagi, H. Gangi, K. Miyagawa, B. Zhou, A. Kobayashi, and K. Kanoda, *Phys. Rev. B* **95**, 224427 (2017).
- [14] R. Takagi, D. P. Sari, S. S. Mohd-Tajudin, R. Ashi, I. Watanabe, S. Ishibashi, K. Miyagawa, S. Ogura, B. Zhou, A. Kobayashi, and K. Kanoda, *Phys. Rev. B* **96**, 214432 (2017).
- [15] C. Rovira, J. J. Novoa, J. L. Mozos, P. Ordejón, and E. Canadell, *Phys. Rev. B* **65**, 081104(R) (2002).
- [16] R. Takagi, K. Miyagawa, M. Yoshimura, H. Gangi, K. Kanoda, B. Zhou, Y. Idobata, and A. Kobayashi, *Phys. Rev. B* **93**, 024403 (2016).
- [17] K. Miyagawa, K. Kanoda, and A. Kawamoto, *Chem. Rev.* **104**, 5635 (2004).
- [18] K. Miyagawa, A. Kawamoto, Y. Nakazawa, and K. Kanoda, *Phys. Rev. Lett.* **75**, 1174 (1995).
- [19] T. Sasaki, *Crystals* **2**, 374 (2012).
- [20] K. Kanoda, *J. Phys. Soc. Jpn.* **75**, 051007 (2006).
- [21] A. Kobayashi, E. Fujiwara, and H. Kobayashi, *Chem. Rev.* **104**, 5243 (2004).
- [22] T. C. Farrar and E. D. Becker, *Pulse and Fourier Transform NMR* (Academic, New York, 1971).
- [23] F. Kagawa, Y. Kurosaki, K. Miyagawa, and K. Kanoda, *Phys. Rev. B* **78**, 184402 (2008).
- [24] T. Furukawa, K. Miyagawa, T. Itou, M. Ito, H. Taniguchi, M. Saito, S. Iguchi, T. Sasaki, and K. Kanoda, *Phys. Rev. Lett.* **115**, 077001 (2015).
- [25] A. Kawamoto, K. Miyagawa, Y. Nakazawa, and K. Kanoda, *Phys. Rev. B* **52**, 15522 (1995).